Single relaxation time model for entropic lattice Boltzmann methods

Santosh Ansumali and Iliya V. Karlin
Department of Materials, Institute of Polymers, ETH-Zürich, ETH-Zentrum, Sonneggstrasse 3, ML J 19, CH-8092 Zürich, Switzerland
(Received 30 March 2001; revised manuscript received 5 March 2002; published 20 May 2002)

For lattice Boltzmann methods based on entropy functions, we derive a collision integral which enables simple identification of transport coefficients, and which circumvents construction of the equilibrium. Implementation of the two-dimensional hydrodynamics demonstrates considerable increase of stability with respect to conventional lattice Boltzmann schemes.

DOI: 10.1103/PhysRevE.65.056312 PACS number(s): 47.11.+j, 05.70.Ln

I. INTRODUCTION

The lattice Boltzmann method (LBM) is a useful approach to simulation of complex macroscopic phenomena in spatially extended systems such as hydrodynamics [1]. In the LBM, macroscopic equations are not addressed directly by a conventional discretization procedure, rather, ''enveloping,'' fully discrete kinetic models are constructed in such a way that (i) their long time, large scale limit matches the macroscopic dynamics in question, and (ii) they are easily implemented numerically. In its present and mostly used form, the LBM is based on (i) a polynomial ansatz with tailored properties for the local equilibrium, and (ii) a single relaxation time model (SRTM) for the relaxation (collision) term. The SRTM has been borrowed from the well known Bhatnagar-Gross-Krook approximation of the Boltzmann collision integral of classical kinetic theory. The resulting method is known as the LBGK model [2,3].

However, in spite of impressive evidence of successful application of the LBM [1], the method is still in the development phase. One of the demanding problems, recognized by many authors, is that of numerical instability [1,4–7].

It has been discussed for some time in the literature [1,4,5,7] that the stability of the LBM could be improved if the method could be based on an analog of the Boltzmann *H* theorem. Theoretical progress in this direction has recently been achieved [4,8]. The essence of this work is as follows: (i) To construct entropy functions whose local equilibria have the desired properties rather than constructing these equilibria approximately, and (ii) to implement the discrete-time *H* theorem for these entropy functions through consideration of pairs of states with equal entropy, and introduction of state-dependent (and hence variable) relaxation times. Although these results are relatively recent, tests have demonstrated the unconditional stability of this class of lattice Boltzmann models (ELBM hereafter) [5,7].

With the entropy-based approach to constructing the lattice Boltzmann models, a different set of problems arises. The most challenging of them is to answer the question: How to implement a single relaxation time model in the framework of the ELBM? Indeed, in many cases, implementation of the ELBM with the BGK collision integral might require numerical evaluation of local equilibria [7]. On the other hand, wide families of admissible collision models can be introduced once the entropy functional is known, which circumvent construction of the local equilibrium explicitly [4]. While the potential richness of these families may be important, it is sometimes crucial to have the simplest, single relaxation time models because identification of transport coefficients is then straightforward. To the best of our knowledge, construction of a SRTM different from the BGK approximation has never been addressed in classical continuous kinetic theory [when the local equilibrium is known explicitly (the local Maxwellian), there is simply no demand for that].

In this paper, we construct a single relaxation time model for the ELBM. This SRTM does not require explicit knowledge of the local equilibrium but the identification of the transport coefficients remains as simple as before. We consider a realization of the ELBM for two-dimensional isothermal hydrodynamics, demonstrating a considerable gain in stability with respect to the classical LBGK method.

II. OVERVIEW OF THE METHOD

In the LBM setup, one considers populations f_i of discrete velocities $\vec{c}_i$, where $i=1,\ldots,b$, at discrete time t. The set of velocities $\vec{\boldsymbol{c}}$ is represented by the links of a regular lattice at each lattice site $\vec{r}$, and it may also include a zero vector. It is convenient to introduce b-dimensional population vectors $\boldsymbol{f}$, and we set $\langle \boldsymbol{x}|\boldsymbol{y}\rangle = \Sigma_{i=1}^{b} x_i y_i$. Local hydrodynamic variables M_k, where $k=1,\ldots,n$, and $n<b$, are defined at each lattice site, $M_k(\vec{r}) = \langle \boldsymbol{m}_k|\boldsymbol{f}(\vec{r})\rangle$, where $\boldsymbol{m}_k$ are corresponding microscopic densities. In the particularly important case of the isothermal hydrodynamics considered below, the microscopic densities are **1** and $\vec{\boldsymbol{c}}$, while the local hydrodynamic variables are

$$\rho = \langle \mathbf{1}|\boldsymbol{f}\rangle, \tag{1}$$

$$\rho\vec{u} = \langle \vec{\boldsymbol{c}}|\boldsymbol{f}\rangle. \tag{2}$$

Vectors orthogonal to $\boldsymbol{m}_k$ are conveniently described in terms of a basis $\boldsymbol{g}_s$ where $s=1,\ldots,b-n$, and $\langle \boldsymbol{g}_s|\boldsymbol{g}_p\rangle = \delta_{sp}$ (the kinetic subspace). Nonhydrodynamic variables $\langle \boldsymbol{g}_s|\boldsymbol{f}\rangle$ correspond to higher-order moments in the context of classical kinetic theory. The basic equation to be solved is

$$\boldsymbol{f}(\vec{r}+\vec{\boldsymbol{c}},t+1) - \boldsymbol{f}(\vec{r},t) = -\frac{1}{2\tau}[\boldsymbol{f}(\boldsymbol{r},t) - \boldsymbol{f}^{\mathrm{eq}}(\boldsymbol{r},t)]. \tag{3}$$

Then a quadratic form for the equilibrium distribution distribution function f^{eq} is used, which reproduces the Navier-Stokes equation up to the order $O(M^2)$. Here M is the Mach number and τ is a parameter related to the viscosity. However, this approach of constructing the equilibrium distribution as a way to get back the Navier-Stokes equation with desired accuracy does not guarantee obeying the H theorem.

III. ENTROPIC LATTICE BOLTZMANN EQUATION

In the entropic lattice Boltzmann method another approach is taken to ensure the H theorem for discrete time. The basic idea is to construct an H function relevant to the dynamics considered and then obtain the full dynamics from the knowledge of the H function. The whole construction of the ELBM is based on the convex nature of the H function. If the function H is Boltzmann-like (the case considered below), then it is defined in the domain of non-negative population vectors. Non-negative population vectors with fixed values of the hydrodynamic variables but different in the nonhydrodynamic variables form the phase space of the model (the kinetic polytope). The description of kinetic polytopes is an interesting problem of linear programming in itself, studied recently in the context of the ELBM [7], and greatly studied in the closely related context of chemical kinetics [9], where it is known as the reaction polytope. Finally, the local equilibrium population vector $\boldsymbol{f}^{\mathrm{eq}}$ is the minimizer of the entropy function H subject to fixed values of local hydrodynamic variables. The generic ELBM is based on the following kinetic equation:

$$\boldsymbol{f}(\vec{r}+\vec{\boldsymbol{c}},t+1)-\boldsymbol{f}(\vec{r},t)=\boldsymbol{\Delta}^{*}[\boldsymbol{f}^{(\vec{r},t)}]. \tag{4}$$

Here the left hand side is the conventional discrete free propagation, while the right hand side is the ELBM collision integral:

$$\boldsymbol{\Delta}^{*}=\beta\alpha[\boldsymbol{f}(\vec{r},t)]\boldsymbol{\Delta}[\boldsymbol{f}(\vec{r},t)]. \tag{5}$$

In this expression, the parameter β is fixed in the interval $[0,1]$, and α is the scalar function of the population vector. The function α ensures the discrete time H theorem, and is the nontrivial root of the scalar nonlinear equation

$$H(\boldsymbol{f})=H(\boldsymbol{f}+\alpha\boldsymbol{\Delta}[\boldsymbol{f}]). \tag{6}$$

Finally, the *bare* collision integral $\boldsymbol{\Delta}$ must satisfy the following set of admissibility conditions: $\langle \boldsymbol{m}_k|\boldsymbol{\Delta}\rangle=0$ for any $\boldsymbol{f}$ (local conservation laws), and $\langle \boldsymbol{\nabla}H|\boldsymbol{\Delta}\rangle\leqslant 0$ for any $\boldsymbol{f}$, where $\boldsymbol{\nabla}H$ is the gradient of H in the space of population vectors (local entropy production inequality). The entropy production inequality must become an equality, and the $\boldsymbol{\Delta}$ must become equal to zero in the case of $\boldsymbol{f}=\boldsymbol{f}^{\mathrm{eq}}$. The structure of the ELBM collision integral (5) can be interpreted as follows. Bare collision integrals are stripped of any relaxation time parameters, and are merely directions in the space of populations, pointing toward the change of state in the collision update. The parameter α defines the maximal step along this direction so that the entropy will not decrease. The combination $(\beta\alpha)^{-1}$ is thus the effective relaxation time in the fully discrete kinetic picture. It should be stressed [4] that in order for the ELBM (4) to recover the desired macroscopic equations, entropy functions cannot be taken as arbitrary but should be found by a separate consideration. We shall come back to this point later on but for the time being the function H will remain unspecified.

IV. COLLISION INTEGRAL

As discussed earlier, there is a class of possible collision integrals from which the desired dynamics can be constructed. For the purpose of identification of the parameter of the macroscopic dynamics (kinematic viscosity in the present case) the BGK approximation is a simple option. However, for any relevant H function, obtaining the equilibrium distribution in an explicit form is a nontrivial problem. This might require solving a minimization problem at each time step [7]. Our idea is to use this potential freedom available in choosing the collision integral and construct a collision integral in such a way that ease of identification of the parameter in the single relaxation time is preserved, while explicit knowledge of the corresponding equilibrium is avoided. The method of constructing such a collision integral is described in this section.

In the LBM, derivation of the transport coefficients is done using the Chapman-Enskog method in the vicinity of the local equilibrium. In this derivation, spectral properties of the linearized collision integral are most important. The linearization of the ELBM collision integral (5) reads

$$\delta\boldsymbol{\Delta}^{*}=\beta\alpha_{\mathrm{eq}}\boldsymbol{L}\delta\boldsymbol{f}. \tag{7}$$

Here $\boldsymbol{L}$ is the linearized bare collision integral, and $\alpha_{\mathrm{eq}}=\alpha(\boldsymbol{f}_{\mathrm{eq}})$ is found upon expanding Eq. (6) at equilibrium to the first nontrivial (quadratic) order. [Note that a substitution of $\boldsymbol{f}^{\mathrm{eq}}$ into Eq. (6) does not give an equation for α_{eq}. This is natural because, by its sense, α_{eq} is a relaxation parameter which can only be specified by considering deviations from equilibrium.] The result reads

$$\alpha_{\mathrm{eq}}=-\frac{2\langle \delta\boldsymbol{f}|\boldsymbol{\nabla}\boldsymbol{\nabla}H(\boldsymbol{f}^{\mathrm{eq}})|\boldsymbol{L}\delta\boldsymbol{f}\rangle}{\langle \boldsymbol{L}\delta\boldsymbol{f}|\boldsymbol{\nabla}\boldsymbol{\nabla}H(\boldsymbol{f}^{\mathrm{eq}})|\boldsymbol{L}\delta\boldsymbol{f}\rangle}. \tag{8}$$

Here $\boldsymbol{\nabla}\boldsymbol{\nabla}H(\boldsymbol{f}^{\mathrm{eq}})$ is the $b\times b$ matrix of second derivatives of the entropy function at equilibrium. Equation (8) suggests that, in general, α_{eq} has a spectrum of values dependent on the direction along which the equilibrium is approached. However, drastic simplification of Eq. (8) happens if $\boldsymbol{L}$ has the projector property:

$$\boldsymbol{L}\boldsymbol{L}=-\boldsymbol{L}. \tag{9}$$

In this case, the relaxation parameter α_{eq} becomes independent of the direction in the kinetic polytope along which the state relaxes to equilibrium. This is the essence of the SRTM, which simply says that all the $b-n$ kinetic variables relax to zero at the same rate. This important property is satisfied, in particular, by the linearized bare BGK collision integral, and it has already been demonstrated elsewhere [8] that in this case $\alpha_{\mathrm{eq}}=2$.

It is important to notice that simplification of the near-equilibrium dynamics with the projector property (9) concerns solely the *linearized* bare collision integral, but does not say anything yet about situations far from equilibrium. There might be many collision integrals which have the same property (9) near equilibrium but are different elsewhere. Our goal is therefore to construct a nonlinear SRTM which, on the one hand, has the desired projector property (9) near equilibrium (and thus is equivalent to the linearized BGK), and, on the other hand, requires only knowledge of the entropy function.

In order to construct the SRTM, we first write the operator $\boldsymbol{L}$ with the property (9) in terms of a given basis of the kinetic subspace $\boldsymbol{g}_s$:

$$\boldsymbol{L}=-\sum_{s=1}^{b-n}|\boldsymbol{g}_s\rangle\langle\boldsymbol{g}_s|. \tag{10}$$

We seek the SRTM within the following family of admissible collision integrals:

$$|\boldsymbol{\Delta}\rangle=-\sum_{s,p=1}^{b-n}|\boldsymbol{g}_s\rangle K_{sp}(\boldsymbol{f})\langle\boldsymbol{g}_p|\boldsymbol{\nabla}H\rangle. \tag{11}$$

Here K_{sp} are elements of a positive definite $(b-n)\times(b-n)$ matrix $\boldsymbol{K}$. The functions K_{sp} may depend on the population vector, and any representative of the family (11) is admissible. A requirement that the linearization of the collision integral (11) equals $\boldsymbol{L}$ (10) uniquely defines the matrix $\boldsymbol{K}$ at equilibrium:

$$\boldsymbol{K}(\boldsymbol{f}^{\mathrm{eq}})=\boldsymbol{C}^{-1}(\boldsymbol{f}^{\mathrm{eq}}),$$

$$C_{sp}(\boldsymbol{f}^{\mathrm{eq}})=\langle\boldsymbol{g}_s|\boldsymbol{\nabla}\boldsymbol{\nabla}H(\boldsymbol{f}^{\mathrm{eq}})|\boldsymbol{g}_p\rangle. \tag{12}$$

Finally, we need to extend the the matrix $\boldsymbol{K}(\boldsymbol{f}^{\mathrm{eq}})$ to arbitrary $\boldsymbol{f}$. This extension is not unique but we suggest the simplest approach, which amounts to replacing $\boldsymbol{f}^{\mathrm{eq}}$ by $\boldsymbol{f}$ in Eq. (12) to give

$$\boldsymbol{K}(\boldsymbol{f})=\boldsymbol{C}^{-1}(\boldsymbol{f}),$$

$$C_{sp}(\boldsymbol{f})=\langle\boldsymbol{g}_s|\boldsymbol{\nabla}\boldsymbol{\nabla}H(\boldsymbol{f})|\boldsymbol{g}_p\rangle. \tag{13}$$

The matrix $\boldsymbol{C}(\boldsymbol{f})$ is symmetric and positive definite for any $\boldsymbol{f}$ (the last statement follows from the strict convexity of the entropy function for any $\boldsymbol{f}$). Then $\boldsymbol{C}^{-1}$ exists for any $\boldsymbol{f}$, and it is straightforward to prove that the resulting matrix $\boldsymbol{K}(\boldsymbol{f})$ is positive definite for any $\boldsymbol{f}$. In this case we find the nonlinear SRTM given by Eqs. (11) and (13), which is the main result of our paper. Notice that the matrix $\boldsymbol{K}(\boldsymbol{f})$, and all the other elements in Eq. (11), are well defined only once the entropy function is known. For our model, $\alpha_{\mathrm{eq}}=2$, and, given that the entropy function H is chosen appropriately [4], all the derivations of the transport coefficients found by the LBGK model remain valid. Indeed, application of the standard Chapman-Enskog analysis to the lattice Boltzmann equation (4) with *unspecified* entropy function H (hence, with unspecified equilibrium $\boldsymbol{f}^{\mathrm{eq}}$) demonstrates that the dissipative terms in the macroscopic equations are proportional to $(1-\beta)/(2\beta)$ in the case of the entropic SRTM, whereas they are proportional to $(\tau-1/2)$ in the case of the standard LBGK collision integral $\boldsymbol{\Delta}_{\mathrm{BGK}}=-(1/\tau)[\boldsymbol{f}-\boldsymbol{f}^{\mathrm{eq}}]$ (see Refs. [5,7] for details of the Chapman-Enskog computation within the ELBM scheme). Now, for the macroscopic equations to have the required form, in the LBGK scheme the equilibrium has to be specified [2,3], whereas in the ELBM scheme the entropy function has to be found. For isothermal hydrodynamics, such entropy functions has been found in Ref. [4]. In particular, for the two-dimensional case considered below, the unique Boltzmann-like entropy function is known [4] such that its equilibrium reduces to the known LBGK equilibrium ansatz [2] in the limit of low Mach number. Therefore, the form of the hydrodynamic equations in the low Mach number limit is the same for both the models (the Navier-Stokes equations). The viscosity coefficient is directly read off from the well known LBGK result [2] through the correspondence $\tau^{-1}=2\beta$, and we have $\nu=c_{\mathrm{s}}^2(1-\beta)/(2\beta)$, where c_{s}^2 is the sound speed squared.

V. SOLVING ESTIMATION EQUATION FOR THE ENTROPY

The next important point concerns solving the nonlinear equation (6). Because the entire ELBM is largely based on convexity of the entropy function, and also because working with Boltzmann-like H functions does not permit any nonpositivity of populations, it is desirable to avoid methods that do not respect positivity and convexity. Our approach is based on a two-side estimate of the location of the nontrivial root of Eq. (6). The upper bound $\alpha_{\max}>0$ is the minimal solution to the equations $f_i+\alpha\Delta_i=0$, $\Delta_i<0$. In geometrical terms, $\alpha_{\max}$ corresponds to the point on the boundary of the kinetic polytope where the ray $\boldsymbol{f}^{(\alpha)=\boldsymbol{f}+\alpha\boldsymbol{\Delta}}$, $\alpha\geqslant 0$, intersects the boundary. Construction of the lower bound $\alpha_{\min}$ was based on earlier general studies of the initial layer problem in dissipative kinetics [11,12]. Specifically, we consider another nonlinear equation:

$$\langle\boldsymbol{\nabla}H(\boldsymbol{f}+\alpha\boldsymbol{\Delta})|\boldsymbol{\Delta}\rangle=0. \tag{14}$$

In geometrical terms, the unique solution to this equation, $\alpha_{\min}$, defines the population vector $\boldsymbol{f}_{\min}=\boldsymbol{f}+\alpha_{\min}\boldsymbol{\Delta}$, which is the minimum entropy state on the ray $\boldsymbol{f}^{(\alpha)}$. Indeed, the minimum condition is the tangency point of the ray to a level of entropy function, which is precisely statement (14). The nontrivial solution to Eq. (6) is strictly in the interval $[\alpha_{\min},\alpha_{\max}]$. In order to evaluate $\alpha_{\min}$, we have applied the quasi-Newton method of Ref. [11] which guarantees successive approximations $\alpha_{\min}^{(n)}$, $n=1,\ldots,$ and for all n it is valid that $0<\alpha_{\min}^{(n)}\leqslant\alpha_{\min}$. Moreover, the first approximation $\alpha_{\min}^{(1)}$ is known analytically [see Ref. [11], Eq. (9)]. Therefore, we have used this estimate, which guarantees that the solution is located strictly inside the interval $[\alpha_{\min}^{(1)},\alpha_{\max}]$. Starting with this estimate, the bisection method is implemented, which guarantees that positivity of populations will not be violated.

VI. CHOICE OF THE *H* FUNCTION

For any dynamics an H function can be constructed using the concept of minimization of the entropy under constraints. In the case of isothermal hydrodynamics the local equilibrium must obey the constraints of mass and momentum conservation [Eq. (1) and Eq. (1)]. For the sake of completeness, we shall recall here the major steps of the derivation for the nine-velocity lattice [4]. For this case the H function to be minimized under the constraints is

$$H=\sum_{l=0}^{8} h_l(f_l), \tag{15}$$

where h_l, $l=0,\ldots,8$, are the set of nine *a priori* unknown convex functions. By using the symmetry of the nine-velocity lattice the number of the unknown functions can be reduced to three functions h_0, h_1, and h_2 corresponding to velocities with magnitudes 0, 1, and 2, respectively. Thus,

$$H=h_0+\sum_{l=1}^{4} h_1(f_l)+\sum_{l=5}^{8} h_2(f_l). \tag{16}$$

We seek an H function such that its minimum $\boldsymbol{f}^{\mathrm{eq}}$ subject to the hydrodynamic constraints [Eq. (1) and Eq. (1)] satisfies the relation for the pressure tensor

$$\sum_{i=1}^{b} c_{i\alpha}c_{i\beta}f_i^{\mathrm{eq}}=\rho u_\alpha u_\beta+\rho c_s^2\delta_{\alpha\beta}, \tag{17}$$

where c_s is the speed of sound, which is a free parameter for the time being. Here for the sake of clarity we have used the component notation. This statement of the problem leads to a set of nonlinear functional equations. In order to solve these equations approximately, we require that Eq. (17) is satisfied up to second order in $\lambda_\alpha c_{i\alpha}$. Here λ_α $(\alpha=1,2,3)$ are Lagrange multipliers corresponding to constraints. The resulting set of differential equations (rather than functional equations) have a solution only if we take $c_s^2=1/3$. The entropy function after solving this set of equations [4] is

$$H=f_0\,\ln\left(\frac{f_0}{8}\right)+\sum_{l=1}^{4} f_l\,\ln\left(\frac{f_l}{2}\right)+\sum_{l=5}^{8} f_l\,\ln(2f_l). \tag{18}$$

As $\lambda^2\sim u^4$, this solution will satisfy Eq. (17) to the order $O(u^4)$ only. Thus the pressure tensor is accurate up to fourth order only. To be specific, the equilibrium pressure tensor has the form

$$P_{\alpha\beta}^{\mathrm{eq}}=\rho u_\alpha u_\beta+\rho c_s^2\delta_{\alpha\beta}+P'_{\alpha\beta}, \tag{19}$$

where $P'_{\alpha\beta}$ is a nonisotropic tensor of order u^4, the Mach number $M=u/c_s$, and the sound speed $c_s=1/\sqrt{3}$. The effective scalar pressure is a function of u^4, in the present case. This u^4 dependence is not surprising. It has been demonstrated in Ref. [4] that expansion of the local equilibrium of the entropy function (18) to the order u^2, neglecting all the higher order terms in u, results in the polynomial local equilibrium of the nine-velocity (D2Q9) model of Ref. [2] with the equilibrium pressure tensor

$$P_{\alpha\beta}^{\mathrm{eq}}=\rho u_\alpha u_\beta+\rho c_s^2\delta_{\alpha\beta}. \tag{20}$$

Thus, after neglecting higher order terms in u, the method is identical to the LBGK method with zero velocity [2], with which we compare the present algorithm in the next section.

VII. SOME NUMERICAL RESULTS

We have implemented the present scheme for the two-dimensional nine-velocity lattice, using the entropy function

TABLE I. Location of vortex centers.

Re	Reference	Primary vortex $(\psi_{\max},X,Y)$	Lower left vortex $(\psi_{\max},X,Y)$	Lower right vortex $(\psi_{\max},X,Y)$
400	[13][a]	(0.1121,0.5608,0.6078)	$(-1.30\times10^{-5}$,0.0549,0.0510)	$(-6.19\times10^{-4}$,0.8902,0.1255)
	[14]	(0.1136,0.5563,0.6000)	$(-1.46\times10^{-5}$,0.0500,0.0500)	$(-6.45\times10^{-4}$,0.8875,0.1188)
	[15]	(0.1139,0.5547,0.6055)	$(-1.42\times10^{-5}$,0.0508,0.0469)	$(-6.42\times10^{-4}$,0.8906,0.1250)
	[16]	(0.1130,0.5571,0.6071)	$(-1.45\times10^{-5}$,0.0500,0.0429)	$(-6.44\times10^{-4}$,0.8857,0.1143)
	Present work[b]	(0.1127,0.5573,0.6049)	$(-1.2\times10^{-5}$,0.0392,0.0353)	$(-6.09\times10^{-4}$,0.8854,0.1215)
1000	[13][a]	(0.1178,0.5333,0.5647)	$(-2.22\times10^{-4}$,0.0902,0.0784)	$(-1.69\times10^{-3}$,0.8667,0.1137)
	[14]	(0.1173,0.5438,0.5625)	$(-2.24\times10^{-4}$,0.0750,0.0813)	$(-1.74\times10^{-3}$,0.8625,0.1063)
	[15]	(0.1179,0.5313,0.5625)	$(-2.31\times10^{-4}$,0.0859,0.0781)	$(-1.75\times10^{-3}$,0.8594,0.1094)
	[16]	(0.1160,0.5286,0.5643)	$(-2.17\times10^{-4}$,0.0857,0.0714)	$(-1.70\times10^{-3}$,0.8643,0.1071)
	Present work[a]	(0.1178,0.5338,0.5648)	$(-2.16\times10^{-4}$,0.08550,0.0797)	$(-1.67\times10^{-3}$,0.8654,0.1149)
	Present work[b]	(0.1178,0.5338,0.5675)	$(-2.18\times10^{-4}$,0.0882,0.0797)	$(-1.68\times10^{-3}$,0.8654,0.1149)
5000	[13][a]	(0.1214,0.5176,0.5373)	$(-1.35\times10^{-3}$,0.0784,0.1373)	$(-3.03\times10^{-3}$,0.8078,0.0745)
	[14]	(0.0921,0.5125,0.5313)	$(-1.67\times10^{-3}$,0.0625,0.1563)	$(-5.49\times10^{-3}$,0.8500,0.0813)
	[15]	(0.1190,0.5117,0.5352)	$(-1.36\times10^{-3}$,0.0703,0.1367)	$(-3.08\times10^{-3}$,0.8086,0.0742)
	Present work[b]	(0.1204,0.5175,0.5350)	$(-1.34\times10^{-3}$,0.0773,0.136)	$(-3.0\times10^{-3}$,0.8056,0.07160)

[a] $M=0.1732$.
[b] $M=0.1299$.

TABLE II. Location of upper left vortex.

Re	Reference	Upper left vortex (ψ_{max},X,Y)
5000	[13]	$(-1.46\times10^{-3}, 0.0625, 0.9102)$
	[14]	$(-1.40\times10^{-3}, 0.0667, 0.9059)$
	Present work	$(-1.40\times10^{-3}, 0.0664, 0.9090)$

Eq. (18). The six-dimensional kinetic subspace has been described in terms of the standard basis given by d'Humières [10]. Inversion of the 6×6 matrix $\boldsymbol{C}$, Eq. (13), has been done analytically.

In the first set of numerical experiments, we have simulated lid driven cavity flow using the present method. Locations of the vortex centers as computed by the present method are compared with previous work [13–16] in Table I and Table II. The grid size used in the present simulation is 320×320, which is comparable to the grid size used in previous computations with the standard LBGK method (the D2Q9 model) [13]. As in previous works, the Reynolds number is defined by the relation $\mathrm{Re}=VL/\nu$, where V is the lid velocity, L is the length of the box, and ν is the kinematic viscosity. The stream function for $\mathrm{Re}=1000$ and $\mathrm{Re}=5000$ is shown in Fig. 1 and Fig. 2, respectively. The comparison (Table I and Table II) demonstrates the ability of the method to give accurate results over a wide range of Reynolds number.

In order to study the stability of the method, we have performed high Reynolds number simulations with a much smaller grid size. It was found that the present method can perform simulations at arbitrary low values of the viscosity (thus, high Reynolds number) without any numerical instability. For example, on a lattice of size 100×100 the LBGK method is unstable for a Reynolds number of 5000 for the velocity of lid $V=0.1$ $(M=0.1732)$ [13,17]. However, the present method was stable even for much coarser grids. On a lattice of size 60×60, we performed the simulation up to $\mathrm{Re}=5000$ with the velocity of the lid $V=0.075$ $(M=0.1299)$. The result (see Fig. 3) shows that the large scale flow patterns are calculated with acceptable accuracy, whereas the resolution of the smaller scale flow patterns is not possible on this coarse grid. This can be attributed to the following facts.

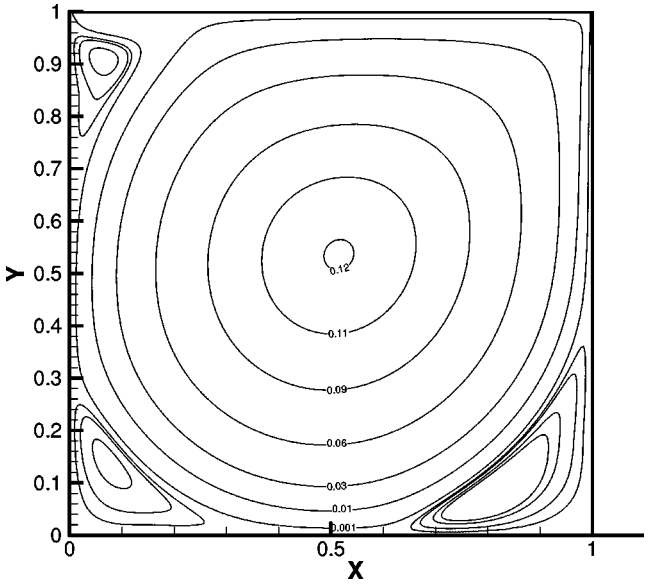

FIG. 2. Stream function for $\mathrm{Re}=5000$ in a simulation of lid driven cavity flow. Parameters used are grid size 320×320; lid velocity $V=0.075$ $(M=0.1299)$. All quantities are given in dimensionless units.

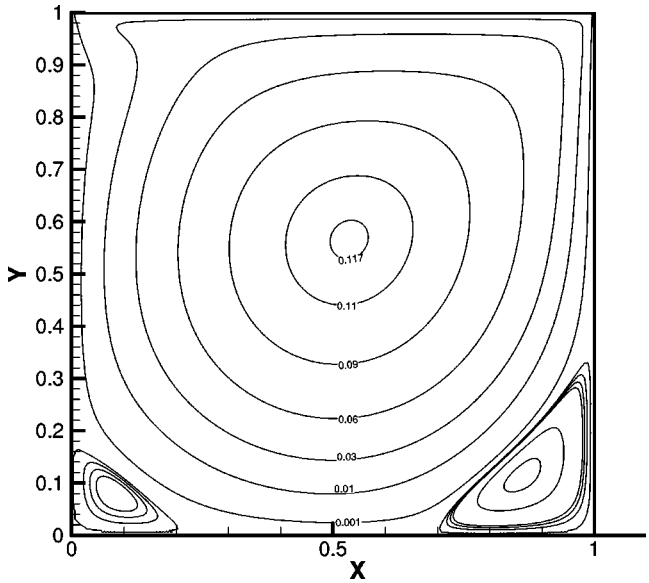

FIG. 1. Stream function for $\mathrm{Re}=1000$ in a simulation of lid driven cavity flow. Parameters used are grid size 320×320; lid velocity $V=0.075$ $(M=0.1299)$. All quantities are given in dimensionless units.

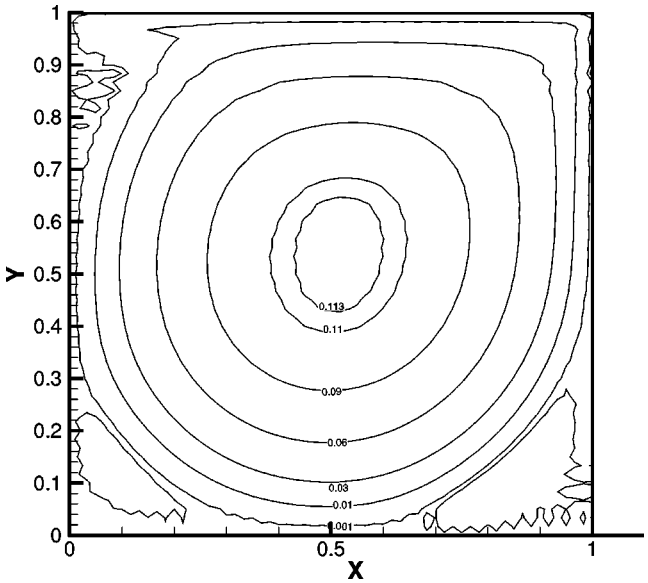

FIG. 3. Stream function for $\mathrm{Re}=5000$ in a simulation of lid driven cavity flow on a coarse grid. Parameters used are grid size 60×60; lid velocity $V=0.075$ $(M=0.1299)$. All quantities are given in dimensionless units.

TABLE III. Mean density fluctuation.

Size	Re	M	Δ_ρ
320×320	1000	0.1732	1.4637×10^{-3}
320×320	1000	0.1299	8.5439×10^{-4}

(1) The lattice is too coarse to resolve the small scale phenomena. This is the reason why the vortices at the corners are more difficult to resolve and the stream function calculated by numerical integration of the velocity is not smooth.

(2) Another problem, again related to resolution, is the large spatial variation of all the quantities in the simulation of high Reynolds number flow on a coarse grid. This problem can be avoided by using higher order spatial discretization schemes for the convection of the distribution function [17].

Decreasing the Mach number results in a more accurate implementation of the incompressibility condition (see Table III). In order to quantify the effect of the compressibility, the mean density and the mean variation of the density are defined as in Ref. [13]:

$$\bar{\rho}=\frac{\int \rho d\mathbf{x}}{\int d\mathbf{x}}, \tag{21}$$

$$\Delta_\rho=\frac{1}{\bar{\rho}}\sqrt{\frac{\int(\rho-\bar{\rho})^2 d\mathbf{x}}{\int d\mathbf{x}}}. \tag{22}$$

Density fluctuations (see Table III) are found to be of the same order of magnitude as in the D2Q9 model [13]. However, the effect of Mach number on the magnitude of the stream function is very small due to the low Mach number used in the lattice Boltzmann method (see the data from the Re=1000 simulation for two different Mach numbers presented in Table I).

In another numerical experiment, the method was extensively tested in setup of the two-dimensional Poiseuille flow, and compared to the standard LBGK (D2Q9) model [1,2]. A lattice with 11×11 nodes was used, with standard bounce-back boundary conditions and standard implementation of the pressure drop [18]. The time evolution of the profile is demonstrated in Fig. 4.

As in the LBGK method without zero velocity and the lattice gas method [3], one can expect that the resulting density distribution in the case of channel flow simulation with the present method will have a higher value at the center of the channel where the magnitude of the velocity is higher. However, this analogy is not complete in the sense that while the error in density in the present case will be of order u^4, it is of order u^2 in the lattice gas or LBGK model without zero velocity. In the simulation we observe that the error due to the bounce-back condition is much larger compared to the

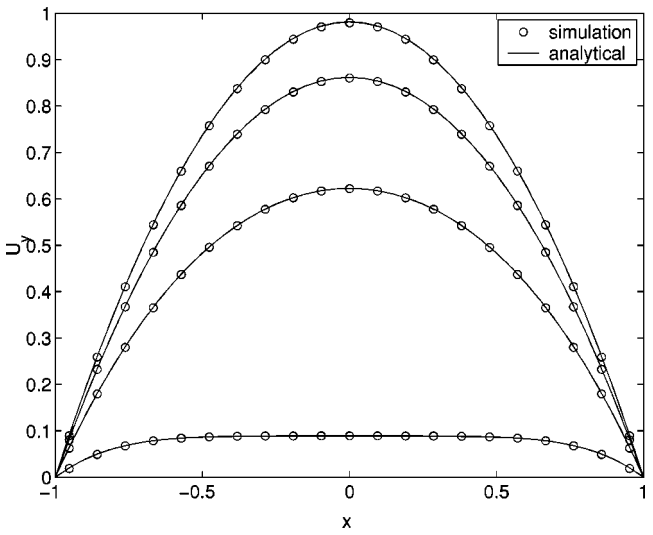

FIG. 4. Development of the velocity profile in Poiseuille flow. Reduced velocity $U_y(x)=u_y/u_{y_{\max}}$ is shown versus reduced coordinate across the channel x. Solid line: analytic solution. Different lines correspond to different instants of the reduced time $T=(\nu t)/(4R^2)$, increasing from bottom to top. Here, R is the half-width of the channel. Symbols: simulation with the present ELBM algorithm. Parameters used are viscosity $\nu=5.0015\times10^{-5}$ ($\beta=0.9997$); steady state maximal velocity $u_{y_{\max}}=1.10217\times10^{-2}$; Reynolds number Re=1157. All quantities are given in dimensionless units.

$O(u^4)$ error inherent in the stress tensor (19) (although the absolute value of the error is quite small). Thus, apart from the error at the boundary, we do not see any other significant error in the density in computations with larger lattices, and on the smaller lattices also the absolute value of the error is quite small (see Fig. 5).

For the same setup as the Poiseuille flow, the stability of both schemes has been investigated with respect to various perturbations. In the first set of tests, nonhydrodynamic perturbations were used, keeping the velocity at each node intact. In particular, populations at all the nodes were perturbed by a small random amount in the same way as was proposed in Ref. [19] for fluctuating hydrodynamics. However, in our case the noise was switched on only at one fixed time t_0, typically after the velocity profile has developed up to its steady state (parabolic) shape. In another set of tests, the fully developed velocity profile was perturbed by adding a small amount of velocity at each node, at time t_0, in a way consistent with the boundary conditions and respecting the incompressibility. In particular, the following perturbations have been used (the origin of the coordinate system is at the central node at the inlet, and the reduced x coordinate $-1\leqslant x\leqslant 1$ is taken across the channel):

$$\delta(\rho u_y)=0.005u_{y\max}\sin(\omega\pi y),$$

$$\delta(\rho u_x)=-0.005\omega\pi x u_{y\max}\cos(\omega\pi y), \tag{23}$$

for all the nodes except for the bounce-back nodes. On the nodes where the bounce-back has been applied, the perturba-

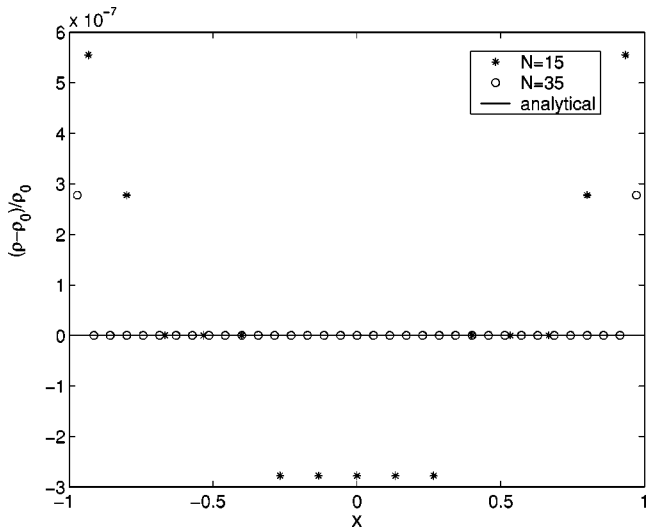

FIG. 5. The error in the density profile in the case of Poiseuille flow. Relative error from the initial density (ρ_0) versus the reduced coordinate across the channel x is plotted for two different lattice sizes ($N=15$ and $N=35$). Parameters used are viscosity $\nu=1.685\times10^{-2}$ ($\beta=0.99$); steady state maximal velocity $u_{y_{\max}}=6.68\times10^{-3}$; reduced time $\tau=0.5$. All quantities are given in dimensionless units.

tion has been set equal to zero, $\delta(\rho u_y)=\delta(\rho u_x)=0$. Perturbations of this type are used quite often in computational fluid dynamics [20].

In both the tests, the excess total kinetic energy $\Delta E(t)=\Sigma_{\boldsymbol{r}}[u^2(\boldsymbol{r},t_0+t)-u^2(\boldsymbol{r},t_0)]$ was monitored for $t\geqslant t_0$. The results are presented in Fig. 6 (random perturbation) and Fig. 7 (velocity perturbation). The present scheme demonstrates

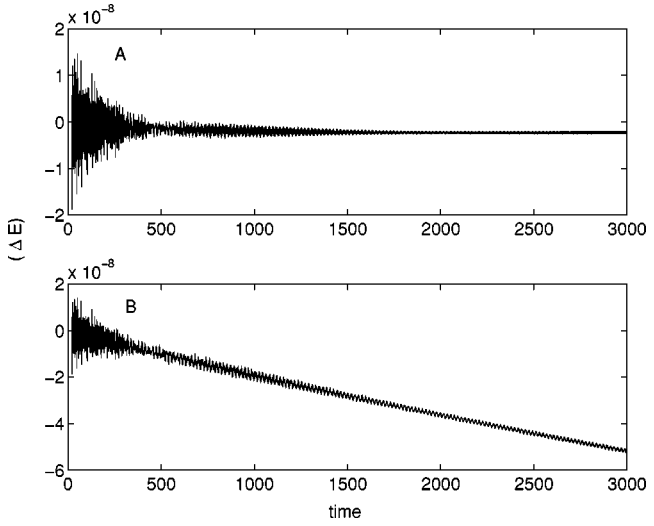

FIG. 6. Time behavior of the excess kinetic energy ΔE after a random perturbation in the population. (a) ELBM, $\nu=8.3752\times10^{-4}$ ($\beta=0.995$), $u_{y_{\max}}=1.8059\times10^{-3}$. (b) LBGK, $\nu=8.3752\times10^{-4}$ ($\beta=0.995$), $u_{y_{\max}}=1.805\,925\times10^{-3}$. The curve terminates after overflow at $t\approx10^5$. All quantities are given in dimensionless units. The excess total kinetic energy $\Delta E(t)=\Sigma_{\boldsymbol{r}}[u^2(\boldsymbol{r},t_0+t)-u^2(\boldsymbol{r},t_0)]$ has been monitored for $t>t_0$.

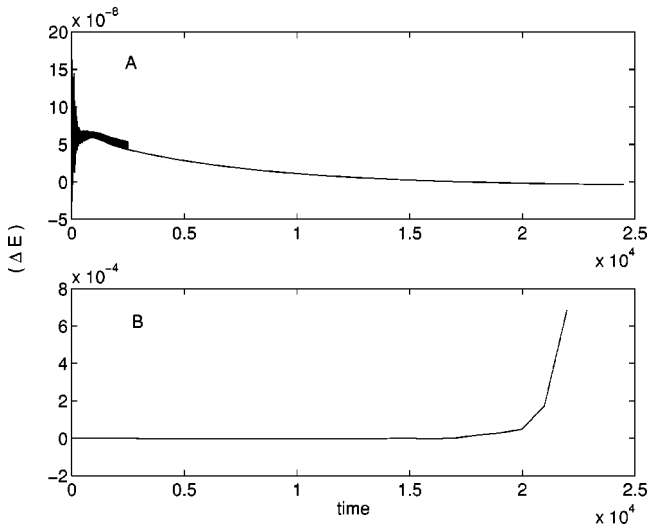

FIG. 7. Time behavior of the excess kinetic energy ΔE after the velocity perturbation (23) with $\omega=3$. (a) ELBM, $\nu=1.683\,502\times10^{-3}$ ($\beta=0.99$), $u_{y_{\max}}=5.390\,55\times10^{-3}$. (b) LBGK, $\nu=1.683\,502\times10^{-3}$ ($\beta=0.99$), $u_{y_{\max}}=5.390\,55\times10^{-3}$. All quantities are given in dimensionless units. The excess total kinetic energy $\Delta E(t)=\Sigma_{\boldsymbol{r}}[u^2(\boldsymbol{r},t_0+t)-u^2(\boldsymbol{r},t_0)]$ has been monitored for $t>t_0$.

the decay of the excess kinetic energy and the return to the unperturbed velocity profile for $\nu_{\min}^{\mathrm{ELBM}}\geqslant10^{-5}$ (the minimum viscosity we used in our tests), whereas $|\Delta E|$ grows in the LBGK scheme, resulting in ultimate numerical overflow for $\nu_{\min}^{\mathrm{LBGK}}<10^{-3}$. The present algorithm is unconditionally stable, and for arbitrary low values of the viscosity never runs into overflow. The implementation of the present model for different flow conditions will be reported elsewhere.

In all the computations with our model, it was found that the hydrodynamic regime sets in rapidly, that is, the actual computed parameter α very rarely deviates significantly from its equilibrium value $\alpha_{\mathrm{eq}}=2$, On the other hand this value is never *exactly* 2 (within machine precision), and switching off the computation of α at each time step by setting it equal to α_{eq} is not possible. The present SRTM with fixed $\alpha=2$ is a ''transient'' model between the entropic LBM and the LBGK: It operates with a fixed relaxation time, but the equilibrium distribution is not yet approximated by the quadratic form; rather, the full entropy-based collision matrix is used. It is not very surprising that this fixation of the relaxation time results in a violation of the H theorem, and leads to numerical overflow, although at values of viscosity lower than in the LBGK scheme. Thus, computation of the parameter α is indeed necessary.

VIII. COMPUTATIONAL COST AND CONVERGENCE OF THE SCHEME

The method of implementation for the entropy estimate described above is quite general. The method can be implemented for any entropy function. However, near local equilibrium α should be very close to 2. This information is used to refine the root solver by using a combination of the Newton-Raphson method and the bisection method [21].

With this modification, the solver usually converges to the root in approximately 10 iterations. This minimizes computational overhead for solving the nonlinear equation.

In general, the ELBM has to perform two extra steps in comparison to the LBGK scheme. The first step is the computation of the bare collision integral, Eq. (13). The second step is to solve the nonlinear equation (6). Both of these operations scale linearly with the number of lattice nodes.

On a Sun workstation for a grid size of 21×21 doing 10, 000 time steps with the present scheme took around 130 s while with the BGK scheme the time involved was around 13 s. A BGK simulation of 10,000 time steps for a grid size of 63×63 took around 120 s. Thus, the present scheme is an order of magnitude slower compared to the BGK method. In the present scheme around 80% of the time is spent evaluating the collision operator. Notice that the collision matrix in the standard LBGK scheme is diagonal and any improvement over the LBGK method has to deal at least with evaluation of a collision matrix of size $(b-M)\times(b-M)$. Here M is the number of conservation laws. One such example is the recently proposed method [6] based on a linear stability analysis. On the other hand, the time required to solve for the entropy estimates contributes only around 5–10 % to the total computation time. This shows that the idea of solving the entropy estimation equation at each time step to ensure the H theorem is computationally not a very heavy burden. This can be implemented easily in an efficient way. However, further progress is needed to reduce the computational cost involved in the calculation of the collision step.

IX. CONCLUSION AND OUTLOOK

In this paper, we have introduced a single relaxation time model for the lattice Boltzmann method based on the entropy function. This model is quite general, and it circumvents difficulties in finding equilibria for the ELBM [7]. The above analysis contributes to the development of the lattice Boltzmann method as the minimal, self-consistent Boltzmann kinetic theory, equipped with the H theorem, and with a realizable collision integral.

After demonstrating that it is viable to incorporate the H theorem into lattice Boltzmann simulations, the focus of the entropic lattice Boltzmann model shifts back to the problem of derivation of entropy functions with tailored properties. The earlier approach [4] based on solving functional equations becomes tedious when the number of constraints goes up, as in the case of the thermal LBGK scheme, for example. Therefore, one needs to think of other possible approaches to derivation of the H function for the thermal case. One possible approach might be based on a modification of the derivation of the lattice Boltzmann method from the continuous Boltzmann equation [22]. Indeed, this derivation is based on Grad's moment method [23], together with the Gauss-Hermite quadrature in velocity space. A different but also well known technique of continuous kinetic theory, closely related to Grad's method, is a velocity polynomial expansion of $\ln f$ (rather than a velocity polynomial expansion of the distribution function f, as in Grad's method) [24,25]. This method, known as the quasiequilibrium approximation (see, e.g., [26]), is consistent with Boltzmann's H theorem: If $\ln f^*(M,\mathbf{v})$ is the approximation, where M are the coefficients in front of the velocity polynomials, then the H function is

$$H(M)=\int \ln f^*(M,\mathbf{v})\exp\{\ln f^*(M,\mathbf{v})\}d\mathbf{v}.$$

Evaluation of this expression with the help of a quadrature is a promising source of H functions for lattice models. This point needs further study, which is left for future work. It should also be mentioned that the quasiequilibrium approximation has recently begug to be exploited systematically for complex fluids such as flexible and liquid crystalline polymer solutions [27]. A combination of quadrature evaluation with these developments may contribute to development of the lattice Boltzmann method for viscoelastic models where the direct approach based on the Boltzmann equation remains problematic [28].

[1] S. Chen and G.D. Doolen, Annu. Rev. Fluid Mech. **30**, 329 (1998).
[2] Y.H. Qian, D. d'Humières, and P. Lallemand, Europhys. Lett. **17**, 479 (1992).
[3] H. Chen, S. Chen, and W.H. Matthaeus, Phys. Rev. A **45**, R5339 (1992).
[4] I.V. Karlin, A. Ferrante, and H.C. Öttinger, Europhys. Lett. **47**, 182 (1999).
[5] S. Ansumali and I.V. Karlin, Phys. Rev. E **62**, 7999 (2000).
[6] P. Lallemand and L.-S. Luo, Phys. Rev. E **61**, 6546 (2000).
[7] B.M. Boghosian, J. Yepez, P.V. Coveney, and A.J. Wagner, Proc. R. Soc. London, Ser. A **457**, 717 (2001).
[8] I.V. Karlin, A.N. Gorban, S. Succi, and V. Boffi, Phys. Rev. Lett. **81**, 6 (1998).
[9] A.N. Gorban, *Equilibrium Encircling* (Nauka, Novosibirsk, 1984).
[10] D. d'Humières, *AIAA Rarefied Gas Dynamics: Theory and Applications*, Progress in Astronautics and Aeronautics, Vol. 159 (Springer, Berlin, 1992), p. 450.
[11] A.N. Gorban, I.V. Karlin, V.B. Zmievskii, and T.F. Nonnenmacher, Physica A **231**, 648 (1996).
[12] A.N. Gorban, I.V. Karlin, and V.B. Zmievskii, Transp. Theory Stat. Phys. **28**, 271 (1999).
[13] S. Hou, Q. Zou, S. Chen, G.D. Doolen, and A.C. Cogley, J. Comput. Phys. **118**, 329 (1995).
[14] S.P. Vanka, J. Comput. Phys. **65**, 138 (1986).
[15] U. Ghia, K.N. Ghia, and C.Y. Shin, J. Comput. Phys. **48**, 387 (1982).
[16] R. Schreiber and H.B. Keller, J. Comput. Phys. **49**, 310 (1983).
[17] R. Zhang, H. Chen, Y.H. Qian, and S. Chen, Phys. Rev. E **63**, 056705 (2001).
[18] X. He, Q. Zou, L.-S. Luo, and M. Dembo, J. Stat. Phys. **87**, 115 (1997).
[19] A.J.C. Ladd, J. Fluid Mech. **271**, 285 (1994).
[20] S.A. Orszag, J. Fluid Mech. **50**, 689 (1971).
[21] W.H. Press, S.A. Teukolsky, W.T. Vettering, and B.P. Flannery,

Numerical Recipes in C (Cambridge University Press, Cambridge, England, 1992), p. 366.
[22] X. Shan and X. He, Phys. Rev. Lett. **80**, 65 (1998).
[23] H. Grad, Commun. Pure Appl. Math. **2**, 331 (1949).
[24] A.M. Kogan, Prikl. Mat. Mekh. **29**, 129 (1965).
[25] M.N. Kogan, *Rarefied Gas Dynamics* (Plenum, New York, 1969).
[26] A.N. Gorban, I.V. Karlin, P. Ilg, and H.C. Öttinger, J. Non-Newtonian Fluid Mech. **96**, 203 (2001).
[27] P. Ilg, Ph.D. thesis, Swiss Federal Institute of Technology, ETH No. 14256, 2001.
[28] A.J. Wagner, e-print cond-mat/0105067.